

Tracking in Aerial Hyperspectral Videos using Deep Kernelized Correlation Filters

Burak Uz Kent*, Aneesh Rangnekar*, and Matthew J. Hoffman**

*Chester F. Carlson Center for Imaging Science, Rochester Institute of Technology

**School of Mathematical Sciences, Rochester Institute of Technology

{bxu2522, apr2635, mjhsma}@rit.edu

Abstract—Hyperspectral imaging holds enormous potential to improve the state-of-the-art in aerial vehicle tracking with low spatial and temporal resolutions. Recently, adaptive multi-modal hyperspectral sensors, controlled by Dynamic Data Driven Applications Systems (DDDAS) methodology, have attracted growing interest due to their ability to record extended data quickly from the aerial platforms. In this study, we apply popular concepts from traditional object tracking—(1) Kernelized Correlation Filters (KCF) and (2) Deep Convolutional Neural Network (CNN) features—to the hyperspectral aerial tracking domain. Specifically, we propose the Deep Hyperspectral Kernelized Correlation Filter based tracker (DeepHKCF) to efficiently track aerial vehicles using an adaptive multi-modal hyperspectral sensor. We address low temporal resolution by designing a *single KCF-in-multiple Regions-of-Interest (ROIs) approach* to cover a reasonable large area. To increase the speed of deep convolutional features extraction from multiple ROIs, we design an effective ROI mapping strategy. The proposed tracker also provides flexibility to couple it to the more advanced correlation filter trackers. The DeepHKCF tracker performs exceptionally with deep features set up in a synthetic hyperspectral video generated by the *Digital Imaging and Remote Sensing Image Generation (DIRSIG)* software. Additionally, we generate a large, synthetic, single-channel dataset using DIRSIG to perform vehicle classification in the *Wide Area Motion Imagery (WAMI)* platform. This way, the high-fidelity of the DIRSIG software is proved and a large scale aerial vehicle classification dataset is released to support studies on vehicle detection and tracking in the WAMI platform.

Index Terms—vehicle tracking, discriminative tracking, hyperspectral sensing, deep features.

I. INTRODUCTION

AERIAL object tracking is a popular topic due to its large range of applications in security, traffic surveillance, autonomous driving, and UAV monitoring. Tracking from aerial platforms can be performed with a number of data modalities including, but not limited to, grayscale [1], thermal [2], color [3] and recently, hyperspectral imagery [4], [5], [6]. Each modality has been exploited for a unique application and comes with its own advantages and disadvantages. In this paper, we will focus on two specific types of sensor modalities: (1) Wide Area Motion Imagery (WAMI), and (2) *adaptive* hyperspectral imagery.

The WAMI platform has enjoyed much attention recently, due to its large area coverage and reasonable spatial resolution. It scans up to a 5km x 5km area at 2 fps where vehicles occupy roughly 100-200 pixels. Such large area coverage becomes possible by employing an array of 6 cameras. Each camera

captures a large field of view single-channel image with slight overlap to the neighboring frame. One can perform persistent tracking utilizing this large field of view image. On the other hand, the low spatial resolution has good performance in vehicle tracking under certain circumstances but is not super helpful when it comes to tackling background clutter, occlusions, and low contrast objects. To counter this, multiple appearance-based features like textures, color histograms, histogram of gradients, and motion cues are used in combination, leading to multiple heat maps for the search area. This is not feasible in real-time tracking as the methods can become computationally expensive and hence there exists a balance between designing complex models vs real-time implementation. Using deep learning techniques in an end-to-end fashion, on the other hand, is not feasible due to availability of the small size datasets captured by WAMI. The datasets recorded by WAMI includes: (1) WPAFB 2009 [7] and (2) CLIF [8] dataset where each one includes a single video with less than 100 frames. Deep learning can be feasible to perform tracking from WAMI with the availability of many more datasets which can take a long time and be very costly. Since data collection from an aerial platform is lengthy and costly, one can utilize deep learning architectures as feature extractors rather than an end-to-end tracking system. In this case, however, WAMI is not a practical platform since it provides single-channel imagery and the deep learning architectures are trained on the large-scale image recognition dataset, ImageNet [9], which uses RGB images.

Due to the availability of rich spectral information that can be recorded by full or adaptive hyperspectral sensors, hyperspectral target tracking from aerial platforms has recently seen increasing popularity [5], [10], [6] as a potential improvement over the WAMI platform. Using this extended spectral information, one can better utilize pre-trained deep architecture in a tracking framework. Also, the use of spectral information can reduce the need to collect higher spatial resolution information. On the other hand, accessibility to a wide spectral range comes with its unique set of challenges, the most important ones being: (1) transmission of massive amount of data on-board the collection platform and, (2) limited temporal resolution. For example, full hyperspectral sensors record hyperspectral channels for the overlooking scene individually. Although very informative, the extremely low temporal resolution and distortion in spectral dimension

prohibits using them for tracking objects. Adaptive hyperspectral sensors are more useful since they they pose a number of advantages over full hyperspectral sensors and can be easily controlled by the DDDAS framework. The Dynamic Data-Driven Applications Systems (DDDAS) framework is very suitable for adaptive sensor control in object tracking to collect the most beneficial data by switching between the sensor modalities. For instance, the *Rochester Institute of Technology Multi-object Spectrometer (RITMOS)* can record data in multiple modalities like panchromatic and hyperspectral data, at comparatively reasonable frame rates by rapidly switching from single-band to hyperspectral modality. This allows the sensor to acquire a wide field-of-view (FOV) panchromatic image followed by a narrow FOV hyperspectral data capture [5], [6]. For the purpose of this study which is more tracking oriented and less control oriented, we refer the readers to [10], [11] for more information on DDDAS inspired sensor control.

A. Motivations

The rich sensory information from hyperspectral imagery has been utilized by *generative* trackers [5], [6]. The *discriminative* and *deep learning* driven trackers on the other hand have recently improved the traditional object tracking dramatically. The main challenges behind the application of discriminative and deep learning trackers in aerial hyperspectral images are:

- Well-established discriminative algorithms such as Efficient Convolutional Operators (ECO) [3], Kernelized Correlation filters (KCF) [12], Struck [13], and Tracking-learning-detection (TLD) [14] are mostly associated with close-angle color image single/multi object tracking at high video frame rates and thus, consider a small ROI.
- The cost of collecting data from aerial platforms makes it hard to find/collect large samples of aerial data, leaving the community to split a single video into training and validation sets [15], [16]. This leads to very optimistic results during off-line tracking due to minimal variance in the training dataset, which results poor performance during online tracking.

B. Contributions

This study addresses the unique challenges posed by the application of discriminative trackers to aerial platforms. We propose a novel method that employs a discriminative tracker that is robust to low temporal (around 1.42 fps) and spatial resolutions (0.3 m). First, we design a method to enlarge the area considered by the tracker to handle the low temporal resolution. Given the rich hyperspectral imagery, we utilize pre-trained deep convolutional networks as feature encoders to boost tracking performance. To accommodate deep features in a near real-time tracking system, we design an *ROI mapping* strategy that only forward-passes the large ROI and projects the individual ROIs to the large ROI feature maps. To the best of our knowledge, this is the first time an adaptive hyperspectral sensor-inspired discriminative tracker (DeepHKCF) has been proposed to perform robust single target tracking in spectral aerial imagery that can be generalized to the

WAMI platform. Finally, we evaluate the proposed tracker on a synthetic hyperspectral video generated by the Digital Imaging and Remote Sensing (DIRSIG) software [17]. To prove the high-fidelity of this video, we synthesize a large single-channel aerial dataset using DIRSIG and train a CNN on it to classify images from the real dataset (WAMI). We refer the readers to following link to access our synthetic vehicle classification dataset (https://buzkent86.github.io/index.html#_Datasets_).

II. RELATED WORK

Our work builds upon the previous work of Henriques *et al.*[18], [12] with Kernelized Correlation Filters (KCF). Having already discussed the lack of development in using discriminative trackers for aerial tracking, we limit our review of related work to the datasets available for aerial vehicle tracking and recent research in WAMI and spectral vehicle tracking.

A review of the related papers indicates that there is limited availability of annotated datasets for aerial tracking in which trackers can be evaluated for their accuracy and robustness. The VIVID [19] is the one of the few publicly available datasets that comes with RGB images, however, it has application limitations due to its relatively small sequence size, low temporal resolution (6 fps), and few occlusions. An upgraded version of this dataset, UAV123, was recently released for research purposes by Mueller *et al.*[20], but the ground sampling distance (GSD) is significantly lower than the high-altitude aerial platforms - thus resulting in objects occupying more than 500-1000 pixels whereas in WAMI platform vehicles are represented by 100-200 pixels. At the same time, the dataset has sequences at 30 fps, drastically higher than standard WAMI/Spectral sequences which are generally in the 1.42 fps - 2 fps range. Since flying RITMOS on an aerial platform is still an ongoing area of development and due to lack of any other real dataset in this area, we use tracking in real world WAMI as a baseline for our approach and then port to using synthetically generated RITMOS-like data to evaluate the performance of our proposed tracker.

A recent survey by Sommer *et al.*[21] showed that a major share of state-of-the-art methods in WAMI moving object detection broadly fall under two categories: 2-frame differencing and background subtraction. Teutsch and Grinberg [22] attempted to track vehicles in WAMI using the former with promising results, however a large number of false negatives still occur during the initial 2-frame differencing for making object proposals. Cormier *et al.*[23] showed that combining Local Binary Patterns (LBP) and Local Variance Measure (VAR) histograms as descriptors, with the usage of Hellinger distance as a measure for similarity, can significantly improve vehicle detection in WAMI data, which can result in superior tracking. Recently, LaLonde *et al.*[15] used a multiple-frame fully convolutional deep model for single and multi-object detection in WAMI videos with great results. On the other hand, there have been few tracking studies using hyperspectral imagery. Uz Kent *et al.*[5] considered the RITMOS platform to perform single target tracking by sampling a narrow FOV region of interest (ROI) hyperspectrally to search for the

target. Using the full frame single-channel image, they remove the global camera motion and couple the narrow-ROI detection and Bayes Filter based tracking modules. Many remote-sensing based processing stages are applied before an HoG-SVM classifier is finally trained to detect vehicles. The proposed approach showed promising results, however they relied on classifiers trained on the same scene to the test video. A more recent approach [6] proposed the adaptive mixture of hyperspectral likelihood maps into a single distance map, thus removing the need for off-line learned classifiers.

III. ADAPTIVE HYPERSPECTRAL SENSING CONCEPT

Single modality electro-optical sensors such as *WAMI* are commonly used for aerial tracking, however, the unique challenges posed by aerial platforms can be better addressed by smarter multi-modal data acquisition. In this direction, the *Rochester Institute of Technology Multi-object Spectrometer* (RITMOS) concept is utilized by a number of trackers [24], [25], [5], [6] as an example of a sensor that can collect a small, targeted amount of hyperspectral data. The RITMOS captures data in two different modalities : (1) full frame single channel image, and (2) limited hyperspectral data from the desired pixel locations. It can acquire a full-frame single channel image in about 0.1 sec and scan a row of pixels hyperspectrally in 1 ms. Such an adaptive and multi-modal data concept provides more freedom to address aerial tracking challenges. Driven by this freedom and specifications, we design a *discriminative* tracker to operate on this platform as shown in Fig. 1. For more information on RITMOS see [26], [5].

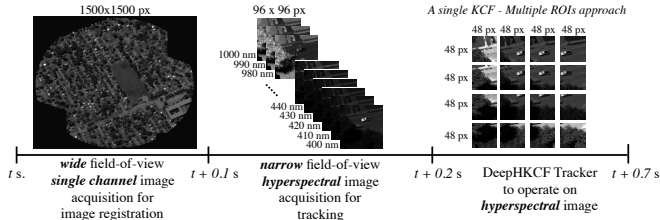


Fig. 1: The proposed Kernelized Correlation Filter driven tracker inspired by RITMOS.

A. Synthetic Scenarios

The *Digital Imaging and Remote Sensing (DIRSIG)* software has been used before to generate spectral scenarios for varied applications that use conventional computer vision techniques and deep learning based models [10], [6], [27], [28]. Since flying spectral sensors on an aerial platform is still an ongoing area of development due to the high costs involved, we evaluate our tracker on synthetic scenarios generated using DIRSIG by [29], [30], [5]. In particular, we will focus on two scenarios : (1) with trees and (2) without trees. We track 43 vehicles in both scenarios similar to the previous studies. One frame from each scenario can be visualized in fig. 2. In addition, we generate a synthetic single-channel aerial dataset for training a CNN and use it to perform vehicle classification on the real WAMI platform, similar to [27] (Sect. V).



(a) 130th frame (with trees) (b) 130th frame (without trees)

Fig. 2: Part of the two frames from the synthetic scenarios generated by DIRSIG. The scene comes from the Mega-Scene 1 area available in DIRSIG. The Mega-Scene 1 area represents part of Rochester, NY.

IV. PROPOSED ALGORITHM

The Kernelized Correlation Filter (KCF) is a well-known single target tracking method that has emerged as a state-of-the-art tracker in the VOC15 tracking benchmark. Its work flow has been detailed in other papers [18], [12]. This section, first, briefly goes over the KCF and document the parts of proposed DeepHKCF tracker later.

The KCF has emerged as a high accuracy tracker that can operate at hundreds of frame rate. Its computational efficiency is derived from the correlation filter framework that represents training examples using a circulant matrix. The fact that a circulant matrix can be diagonalized by Discrete Fourier transform is the key to reducing the complexity of any tracking method based on the correlation filter. The off-diagonal elements become zero whereas the diagonal elements represent the eigenvalues of the circulant matrix. The eigenvalues are equal to the DFT transformation of the base sample (x) elements. The Kernelized Correlation Filter, in particular, applies a kernel to x to transform the feature channels to a more discriminative domain. The circulant matrix is then formed by applying cyclic shifts on the kernelized x . This kernelization operation maintains $O(n \log(n))$ complexity unlike other kernel algorithms which are $O(n^2)$.

Essentially, the KCF solves the problem of regression in the form of the regularization (ridge regression):

$$E(h) = \frac{1}{2} \|y - \sum_{c=1}^C h_c * x_c\|^2 + \frac{\lambda}{2} \sum_{c=1}^C \|h_c\|^2 \quad (1)$$

where y represents the desired continuous response whereas h and x_c represent the learned correlation filter and the training template for the given channel. The parameter c enables one to integrate features in multiple channels, such as HoG and color, in this setup [12], [31]. A closed-form solution for Equation 1 exists. To reduce the complexity of the closed-form solution, an element-wise multiplication in the frequency domain was proposed for \hat{w} :

$$\hat{w} = \hat{x}^* * \hat{y}(\hat{x}^* * \hat{x} + \lambda)^{-1}. \quad (2)$$

A non-linear version of this closed-form solution addresses further geometric and photometric variations [12]. The diago-

normalized Fourier domain dual form solution (non-linear version) is expressed as

$$\hat{\alpha} = \hat{y}(\hat{k}^{xx} + \lambda)^{-1}, \quad (3)$$

where \hat{k}^{xx} represents the first row of the kernel matrix K known as *gram matrix* and is formulated as

$$k^{xx'} = \exp\left(-\frac{1}{\alpha^2}(\|x\|^2 + \|x'\|^2 - 2F^{-1}\left(\sum_c \hat{x}_c^* \odot \hat{x}'_c\right))\right). \quad (4)$$

An earlier version based on this formulation employed grayscale feature ($C = 1$) to learn the solution vector w (MOSSE). Later, multi-channel features such as HoG, Color, and a concatenation of them showed improved accuracy [12], [31], [32], [33], [34]. Once the kernel is learned, one can execute an object detection with multi-channel features as

$$r(z) = F^{-1}(\hat{k}^{xz} \odot \hat{\alpha}), \quad (5)$$

where r denotes the correlation response at all cyclic shifts of the first row of the kernel matrix.

The temporal information can be further integrated into the KCF by updating the filter at every frame as follows.

$$\hat{\alpha}_t = \beta \hat{\alpha}_t + (1 - \beta) \alpha_t \hat{\alpha}_{t-1}. \quad (6)$$

This correlation filter framework only estimates the translation of the object whereas the scale of the object can be updated by running a correlation filter on different size ROIs with same centroids [35]. By correlating a filter with different ROIs, we can get multiple response maps and choose the one with highest confidence to estimate the new scale of the target. In this study, we do not estimate the scale of the target as the scenarios are captured from a fixed altitude platform.

A. Single KCF-Multiple ROIs Approach

Discriminative trackers like KCF learn to function in an online manner by collecting positive and negative samples and then detecting the target of interest in a ROI to update the classifier. Unfortunately, the discriminative features required for KCF to function well are hard to collect from aerial imaging platforms due to their low spatial resolution.

The vanilla-form KCF requires relatively small ROIs, as the appearance-based features deteriorate with larger background context in the ROI. An area as big as three times the size of the target is considered in vanilla-form KCF. Increasing the context size leads to background dominated features, resulting in confusion between different objects. Unfortunately, the platform we consider has lower temporal resolution (1.4 fps) than the other aerial platforms, leading to large displacement of objects in successive frames. Adding the platform motion into this picture makes the application of vanilla-form KCF in aerial platforms extremely difficult.

To handle these challenges, we propose a single KCF-in-multiple ROIs approach as shown in fig. 3. Our approach applies the same KCF to different ROIs overlapping each other to minimize the likelihood of target loss. It is essential to have reasonable overlap between the ROIs (sect. VI-F) as we filter each ROI with a hanning window to avoid distortion

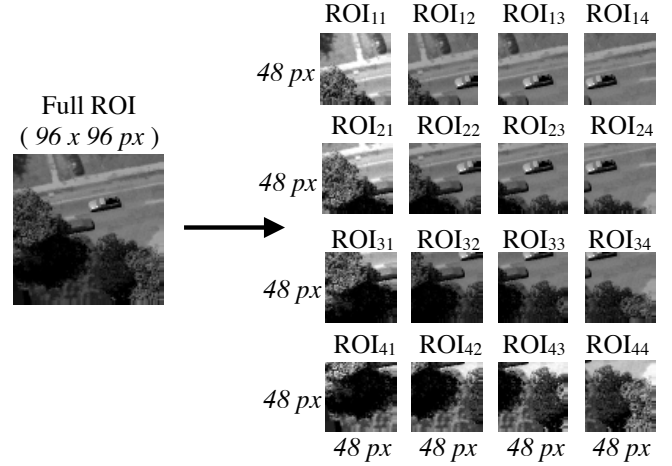


Fig. 3: The proposed single KCF - multiple ROI approach to enlarge the ROI to overcome large displacement of vehicles in low resolution data. The vehicle of interest is shown in yellow rectangles.

at boundaries due to *FFT* operation. This approach can be formulated as

$$r(z_{ij}) = F^{-1}(\hat{k}^{xz_{ij}} \odot \hat{\alpha}) \quad (7)$$

where i and j represent the indexes for different ROIs. A simple way to estimate the new position of the target in this framework would be using the peak-to-side-lobe (PSR) values in ROIs and finding the position of the pixel with maximum confidence in all ROIs as

$$r(z_{final}) = \underset{i,j \in \sqrt{m}}{\operatorname{argmax}}(\operatorname{PSR}(r(z_{ij}))) \quad (8)$$

where m represents the number of ROIs in full ROI. The *PSR*, on the other hand, denotes the margin between the peak value in the response map and the mean of the sidelobe corresponding to the area excluding the 11×11 pixels around the peak. The result is normalized by the standard deviation of the sidelobe as follows.

$$\operatorname{PSR}(r(z_{final})) = \frac{\max(r(z_{final})) - \mu_{\text{sidelobe}}}{\sigma_{\text{sidelobe}}} \quad (9)$$

This position estimation approach can be softened by considering all the ROIs with PSR values larger than a pre-determined threshold. In this case, the formulation can be reorganized as follows.

$$r(z_{final}) = \sum_i \sum_j^{\sqrt{m}} \beta_{ij} * r(z_{ij}), \quad (10)$$

$$\beta_{ij} = \begin{cases} 0, & \text{if } \operatorname{PSR}(r(z_{ij})) > T \\ \operatorname{PSR}(r(z_{ij})), & \text{otherwise.} \end{cases} \quad (11)$$

By softening our decision, we perform low-pass filtering and avoid jumps to other objects that has a high PSR value in only one ROI.

As mentioned earlier, the single KCF-multiple ROIs approach can better handle the low temporal resolution than the traditional KCF. On the other hand, it increases the

complexity linearly to $O(m \cdot n \log(n))$ from $O(n \log(n))$ where m represents the number of ROIs in the full ROI. The low temporal frame rate of the scenario helps us accommodate this approach in the DeepHKCF tracker. One can further increase the frame rate by running the KCF on the multiple ROIs in parallel as ROI operations are independent.

B. Traditional Low-level Features

Tracking-by-detection algorithms exploit low-level features such as Histogram of Oriented Gradients and Color-naming features [36], [35], [37] to perform discriminative tracking until the emergence of deep CNN architectures in the computer vision field. The first correlation filter tracker, MOSSE [38], used a grayscale channel to learn the classifier vector. Following the MOSSE tracker, a correlation filter accommodating multi-channel features was proposed to boost tracking. Later, the SAMF tracker [35] was proposed to concatenate multi-channel HoG and color-naming features. Finally, a kernelized version of correlation filter (KCF) using multi-channel features was proposed to further improve tracking without drastically increasing the computational complexity. In this study, we follow the KCF tracker and concatenate multiple features as in the SAMF tracker. More specifically, we concatenate the HoG feature channels and pure hyperspectral channels and apply Gaussian kernel operation to learn a more discriminative model as follows

$$k^{xz'} = \exp\left(-\frac{1}{\alpha^2}(\|x\|^2 + \|x'\|^2 - 2F^{-1}\left(\sum_{C_{HoG}=1}^{C_{HoG}} \hat{x}_{c_{HoG}}^* \odot \hat{z}'_{c_{HoG}} + \sum_{C_{HSI}=1}^{C_{HSI}} \hat{x}_{c_{HSI}}^* \odot \hat{z}'_{c_{HSI}}\right)\right) \quad (12)$$

where C_{HoG} and C_{HSI} represent the number of channels in HoG features and hyperspectral data. For hyperspectral channel features, we use all 61 bands provided by the RITMOS platform in the ROI. To complement spectral features with shape features, we utilize the fHoG features proposed by [37]. The fHoG features provide 31 feature channels where channels specialize in different orientation bins computed over the gradients in *red*, *green* and *blue* channels. To sum up, the KCF tracker with traditional features learns a model over the Gaussian-kernelized space of 91 dimensional feature channels.

C. Deep Convolutional Features

Convolutional Neural Networks have enjoyed enormous popularity in the computer vision/machine learning community following the emergence of large-scale datasets such as ImageNet. They have surpassed the state-of-the-art methods in all the computer vision/machine learning domains, thanks to their capability to learn varying levels of feature abstractions. Similar to image classification and object detection, the benchmark performances for object tracking have improved dramatically over the last few years.

The first studies utilizing CNN architectures in object tracking focused on employing the features learned in architectures such as AlexNet [39], VGGNet [40] and GoogleNet [41] trained on the ImageNet large scale image classification

dataset [9]. [42] extracted low-level features from VGGNet to learn a more discriminative correlation filter. Specifically, they encoded objects with the activations of the first several convolutional layers from VGGNet. This setting provided them with a 64x64x96 dimensional low-level feature set that can be interpreted as a more advanced version of HoG features. They reported slight improvement in the VOC15 object tracking challenge with deep CNN features over the HoG features. Going deeper is a major key to achieving the state-of-the-art in most computer vision challenges, however, the nature of deep CNN architectures prohibits us from applying high-level features in tracking-by-detection algorithms. This is mainly due to increasing *translation invariance* in deeper layers resulting from spatial pooling operations. [43] proposed a hierarchical multiple KCFs tracking framework accommodating a higher level of feature encodings with CNNs. Their method first employs the activations of the fifth convolutional layer to perform a coarse target search. In the next stage, they use mid-level features computed over the position estimated in the first step to fine-tune the estimated position. In the final step, low level features are extracted from the previously estimated position to further fine-tune the estimate.

The object tracking community later migrated to training architectures to perform object tracking in an end-to-end framework [44], [45], [46]. In this direction, *Siamese Networks* have gained the reputation of the most efficient and effective architecture in tracking. Two branches consisting of the same architecture layers are used in a typical Siamese Network. The bottom branch is provided the ground truth of an object of interest in an ROI, whereas the top branch is assigned the task of estimating the position of the object given the new ROI. Late fusion of the branches is performed and the new position is predicted. The Siamese Networks have surpassed all the other deep tracking-by-detection algorithms in the VOC15 challenge, however, the lack of aerial datasets prohibits us from applying these networks to the aerial tracking domain. For this reason, we believe that, at this stage, it is more practical to use the CNN architectures as feature extractors in aerial platforms where we have RGB data.

In this study, we follow an approach similar to [42] to learn a discriminative model for the KCF as shown in fig. 4. Thanks to low spatial resolution in our scenario, we can pursue a slightly higher level of abstraction of objects. In particular, we apply the activations of the fifth convolutional layer learned in VGGNet [40] trained over ImageNet [9]. Additionally, we experiment with different levels of object abstractions in the results section.

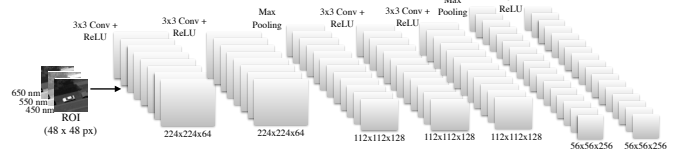


Fig. 4: The proposed feature extraction scheme in the deep hyperspectral kernelized correlation filter tracker. In this figure, the first 5 convolutional layers of the VGGNet [40] are considered.

DIRSIG imagery provides us with a full-frame grayscale image as well as a narrow field of view hyperspectral image at 1.42 fps. Unlike other aerial platforms, it provides hyperspectral data in the visible wavelength range, enabling the use of deep CNN architectures trained on ImageNet consisting of RGB images. One can pick the central *red*, *green* and *blue* channels and forward-pass them through the layers of interest. Another approach could be computing the average of *red*, *green* and *blue* channels in their respective range to come up with the representative red, green and blue channel images to feed the CNN. Our experiments favor the first approach as the latter approach could introduce undesired noise due to the averaging operation.

1) *Fast Convolutional Features with ROI Mapping*: The single KCF-multiple ROIs approach treats each ROI independently to compute the filter response. This requires forward-passing individual ROIs through the CNN architecture as shown in fig. 4. Such an inefficient approach leads to a slower tracker. To increase the run-time performance and perform near real-time tracking at the platform frame-rate, we use the ROI mapping strategy commonly used in convolutional object detectors such as Fast R-CNN [47], Faster R-CNN [48], and R-FCN [49]. This way, we only forward-pass the full ROI and project the individual ROIs to the feature maps extracted from the full ROI as shown in fig. 5.

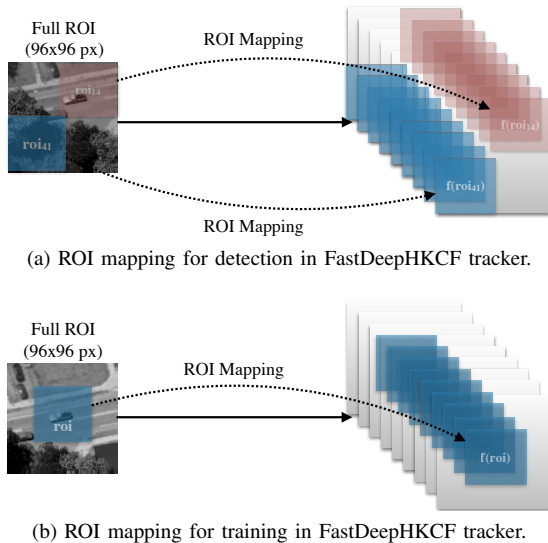


Fig. 5: Proposed ROI mapping strategy to avoid individual ROIs forward-passing through the convolutional network.

With the ROI mapping method, eqns. 7 and 10 can be replaced with the following formulations to perform detection in the FastDeepHKCF tracker.

$$r(f(dROI, droi_{ij}, z)) = F^{-1}(\hat{k}^{x f(dROI, droi_{ij}, z)} \odot \hat{\alpha}), \quad (13)$$

$$r(z_{final}) = \sum_i \sum_j \beta_{ij} * r(f(dROI, droi_{ij}, z)) \quad (14)$$

where $dROI$ represents the full detection ROI used to get the convolutional features z . The individual detection ROIs, $droi_{ij}$, are then projected to the feature map, z , through the projection function f .

Once we estimate the translation of the target, we update the filter using the Fourier domain solution as in eqn. 3. First, the 96x96 px neighborhood around the target is considered and forward-passed through the convolutional network as shown in fig. 5b. To match the detection ROI size (fig. 5a), we then project the central 48x48 px area to the feature maps and reformulate the solution as

$$\hat{\alpha} = \hat{y}(\hat{k}^{f(tROI, troi, x)} + \lambda)^{-1} \quad (15)$$

where $tROI$ and $troi$ represent the full training ROI and actual training ROI mapped to feature maps of the $tROI$ using the function f . On the other hand, we can avoid forward-passing the training ROI if the actual training ROI, $troi$, is a subset of the detection ROI, $dROI$. In this case, the Fourier domain solution can be reformulated as

$$\hat{\alpha} = \hat{y}(\hat{k}^{f(dROI, troi, z)} + \lambda)^{-1}. \quad (16)$$

V. VEHICLE CLASSIFICATION IN WAMI PLATFORM BY USING A SYNTHETIC DATASET

As discussed in Sect. I, detecting cars with high accuracy is a major component of tracking algorithms utilizing the WAMI platform. Unsurprisingly, object detection in traditional images has improved rapidly over the last five years with the emergence of deep learning. To prove this, the state-of-the-art detection accuracy in the PASCAL VOC07 dataset increased from 35% accuracy to over 85% accuracy. However, this dramatic increase is not the case in vehicle detection from the aerial platforms (WAMI). This is due to two major reasons: (1) the lack of a large dataset captured from the WAMI platform and (2) the lack of color channels prevents smooth transfer learning from the networks trained on the ImageNet. In this study, we build a synthetic single-channel vehicle classification dataset using *DIRSIG* and fine-tune a CNN to perform vehicle classification on the real platform (WAMI). By building this dataset, the car detection/classification from the WAMI platform will require a smaller number of samples from WAMI. This also proves the high fidelity of hyperspectral videos used to evaluate the DeepHKCF tracker.

To build such a large-scale dataset, we generate full-frame hyperspectral images captured from the *Mega-Scene-1* scene available in *DIRSIG* [17] with different settings. The simulation setting is designed as a function of *time*. We keep the other parameters similar to the simulation used to generate the RITMOS-like scenario. Overall, nine different simulations are generated from the same scene with the same vehicular traffic and platform motion to the tracking video. One can generate as many simulations as desired, however, we believe that given the aforementioned settings we can generate reasonable number of vehicle and background samples in nine simulations.

A. Temporal Data Augmentation

To keep things manageable, one can generate one frame per simulation mentioned in the previous section. However, then, we need to increase the number of simulations by adding more temporal-variance and changing the initial platform

location. Changing the platform location in a large number of simulations can be a tedious task, thus, to avoid that, we perform temporal data augmentation by generating low frame rate videos on a moving platform. More specifically, the frame rate for each simulation is set to 0.2 fps, resulting in 20 images per simulation. This way, we can capture cars from different angles with different backgrounds.

B. Hyperspectral Data Augmentation

The data augmentation is highly important in our case as we mimic the WAMI platform in a dataset consisting of fully synthetic images. In particular, it is difficult to approximate the spectral sensitivity curve of a real platform synthetically. In this direction, the same car samples from different wavelengths are augmented to better approximate the WAMI platform internal mechanics.

Similar to our tracking video simulation, we stick with 61 channels in the *visible* (400 nm) to *near infrared* (1000 nm) wavelength range. In a single-band image setting with 0.2 fps, we produce about 180 images leading to small spectral variance in the dataset. By using all 61 channels, we generate over 1000 images over the 9 simulations, considering *time* and *spectral* depth. This approach has the potential downside of generating to a dataset dominated by highly similar images. To address this, we sample 6 bands from 6 uniform distributions covering the 61 channels as shown in fig. 6. This increases the spectral variance while ensuring a reasonably large gap between the augmented images at different wavelengths.

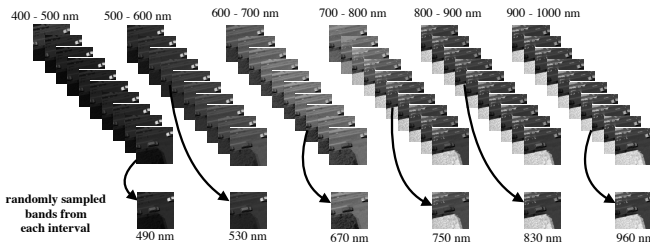


Fig. 6: The proposed hyperspectral data augmentation to increase spectral variance in the dataset. One can observe the variance in the same sample at reasonably distinct wavelengths.

C. Positive and Negative Samples Collection

The procedure described above produces about 27613 vehicle chips, where each chip is cropped from 48x48 pixels area. The vehicles are located in the central position of the positive chips. In our scenarios, similar to the WAMI platform, a vehicle is on average represented by 20x10 pixels. Adding context in positive samples seems to improve the learned weights in a CNN [16]. To collect negative samples, we perform hard-negative mining by considering areas surrounding the positive samples. We randomly sample from an area whose center is $T=10-30$ pixels away from the center of the positive sample.

Our final dataset consists of 55226 chips captured from different positions of *Mega-Scene 1* at different times. To

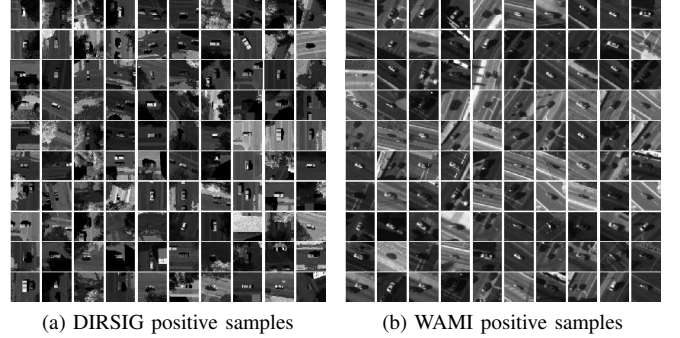


Fig. 7: Positive training samples collected in the DIRSIG vehicle classification dataset and real platform validation samples collected from the WAMI platform (*CLIFF06* and *CLIFF07*) videos.

validate the performance on the WAMI platform, we annotate 600 positive and negative chips from the *CLIFF06* and *CLIFF07* videos captured from the WAMI platform. Some of the positive samples from the training and validation dataset can be visualized in fig. 7. Finally, we train a well-known CNN architecture to perform vehicle classification on the WAMI platform.

The architecture used in this study is the ZFNet, an optimized version of AlexNet. We adapt two different training strategies : (1) training from scratch and (2) fine-tuning the weights learned on the ImageNet using the synthetic aerial vehicle detection dataset. In the latter approach, the learning rate is set to 0.0001 other than the classification layer. The classification layer is assigned 0.0005 learning rate. On the other hand, in the former method, we tune the learning rate to 0.1. The ZFNet from scratch is trained for 4200 iterations with the batch size of 64 whereas the one pre-trained on ImageNet is trained for 400 iterations with the same batch size. In this two experiments, the networks are validated on the 600 samples from WAMI (*CLIFF06* and *CLIFF07*). To integrate further context information into the learned weights, we introduce dilated convolutions with hole size 2 and 1 in the *1st* and *2nd* convolutional layers [50]. Finally, we follow a two-stage training strategy that uses the 200 WAMI samples to further update the weights from the fine-tuned ZFNet. The model is validated on the remaining 400 WAMI samples. This, as expected, boosts the classification accuracy on the WAMI platform. Training is performed on the NVIDIA Tesla K80 GPU in Caffe framework [51].

Method	ZFNet from Scratch	ZFNet (ImageNet)	ZFNet*	AlexNet - WAMI [16]
Accuracy	93.20	92.230	97.0	97.1

TABLE I: Performance of the trained neural networks on the WAMI vehicle classification task. In the "*" case, 200 WAMI samples are used to further fine-tune and validate the network on the 400 WAMI samples. [16] splits the WPAFB2009 video (WAMI) into training and validation.

As seen in table I, over 93% accuracy is achieved by only using our synthetic dataset to train the ZFNet. This proves the

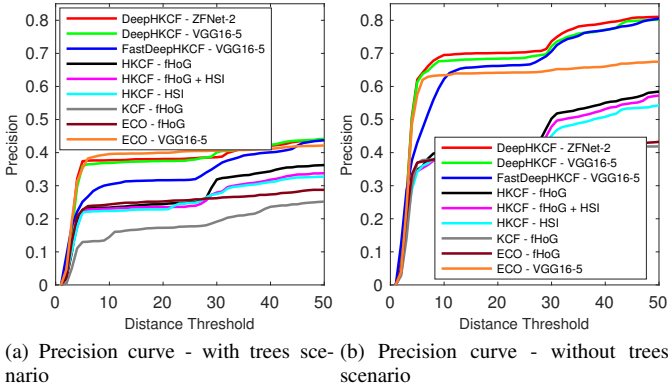


Fig. 8: Precision curves of the DeepHKCF tracker and its variants on the *DIRSIG* scenario with trees and without trees. The ZFNet-2 and VGGNet-5 refer to the activations of the 2nd and 5th convolutional layers.

and about 20% worse in terms of the precision at 50 px and central location error. All in all, the DeepHKCF tracker with ROI mapping (FastDeepHKCF) provides the best tracking results due to its reasonably high tracking accuracy and highest operation rate among the DeepHKCF trackers. What is more, the proposed tracking strategy can be coupled to an advanced KCF tracker such as ECO to further improve tracking.

C. Results on the Scenario with Dense Trees

In addition to conducting experiments on the no-trees scenario, we run the DeepHKCF tracker on the same scenario with *dense trees*. This is an extremely challenging scene dominated by large trees and their shadows as shown in fig. 2. On average, 1 out of 4 frames a vehicle is fully occluded in this video. The occlusions combined with the low frame rate makes this a very challenging scene. The DeepHKCF trackers outperform the other baseline methods other than ECO tracker by a large margin as in the no-trees scenario (fig. 8a). At 20 px precision, the DeepHKCF tracker achieves about 39% accuracy whereas others perform 10-20% worse. On the other hand, among the DeepHKCF trackers, the FastDeepHKCF, delivers similar precision at 50 px and higher frame rate. Interestingly, the combination of hyperspectral feature channels with fHoG degrades the performance with respect to the fHoG-only features. We believe that this could be due to more frequent switching to non-vehicle objects with similar hyperspectral features to target the through occlusions. By using fHoG-only features, it is less likely to switch to an object that does not appear like a vehicle.

The dramatic drop in precision rates between the no-trees and dense trees scenarios is easily seen in fig. 8. This is likely due to three major reasons : (1) high frequency of severe occlusions, (2) low video frame rate, and (3) relatively smaller search area considered by our single KCF-multiple ROIs approach. The combination of the first two reasons leads to dramatically large displacement of objects in between the frames where they are visible. This results in the targets located out of the search area of the DeepHKCF tracker.

There are two solutions to address the challenge of tracking through severe occlusions. The first and less practical solution, is increasing the full ROI size in each dimension. This way, we increase the likelihood of keeping the target in our search area traveling through severe occlusions. However, this will also reduce the run-time performance. A more practical solution could be delivered by leveraging a Bayes Filter. For instance, [6], [4] uses a Bayes Filter in a Multi-dimensional Assignment algorithm to update the measurements in light of the later measurements in the same scenario. This way, we can low-pass the unlikely jumps that occurs during severe occlusions. On the other hand, we believe that, increasing the search area in a practical manner might be the key to achieving state-of-the-art performance in scenarios dominated by trees (see sect. VI-G).

D. Experiments on Temporally Down-sampled Video

In the previous section, we evaluated the proposed trackers and the baseline methods on the 1.42 fps videos with dense trees and without trees. The ECO tracker, the winner of the VOT16 object tracking challenge, performs only slightly worse to the DeepHKCF trackers at 20 px precision. We believe that this might be due to slowly moving or stopped vehicles. To further test the ECO and FastDeepHKCF's performance with respect to more drastic target motion, we down-sample the *video without trees* temporally by *two*, resulting in 0.7 fps video. All the hyperparameters in the FastDeepHKCF and ECO are kept same as before for fair comparison. As seen in table III, the DeepHKCF trackers outperform the ECO tracker by a large margin in terms of precision and central location error, showing its robustness to extreme target displacement in successive frames. The ECO, on the other hand, misses more targets due to the smaller ROI considered in the detection operation.

E. Comparison with Hyperspectral Trackers

Finally, we compare the DeepHKCF tracker, a tracking-by-detection algorithm, to the template-matching based hyperspectral video trackers [6], [5], [4]. These trackers are the state-of-the-art trackers for the *DIRSIG* scenarios. [4] (HFAT) performs median filtering based background subtraction to detect motion, and uses a Bayes Filter to perform predictive hyperspectral sampling to detect stopped vehicles. They assign hyperspectral and kinematic scores to each detected blob and uses the multi-dimensional assignment algorithm to optimally assign the blobs to target. The proposed idea is better suited to fixed camera platforms due to the parallax effect introduced by registration in the moving platforms. [6] propose a generative tracker (HLT) consisting of detection and tracking modules.

Method	DeepHKCF - VGGNet-5	FastDeepHKCF - VGGNet-5	ECO - VGGNet-5
Pr. (20px)	44.34	39.11	29.79
Pr. (50px)	53.30	47.67	34.29
CLE	156.98	174.53	204.85
FPS	0.51	1.11	1.12

TABLE III: Performance of the DeepHKCF and ECO trackers on the temporally down-sampled no-trees video (0.7 fps).

Method	— Best DeepHKCF - ZFNet-2	— 2 nd Best FastDeepHKCF - VGGNet-5	— 3 th Best HFAT [4](6D)*	HFAT [4] (2D)*	HLT [6] (5D)	HLT [6] (2D)
Pr. (20px) - Trees	38.08	31.71	57.63	39.12	51.69	41.86
Pr. (20px) - No-trees	70.13	66.26	N/A	N/A	64.42	57.25
Pr. (50px) - Trees	43.83	44.01	N/A	N/A	55.12	46.72
Pr. (50px) - No-trees	81.05	80.27	N/A	N/A	71.27	68.31
CLE - Trees	156.74	143.66	N/A	N/A	135.03	158.12
CLE - No-trees	48.97	51.71	N/A	N/A	65.36	91.97
FPS	0.51	1.11	1.42	2.32	1.01	1.09

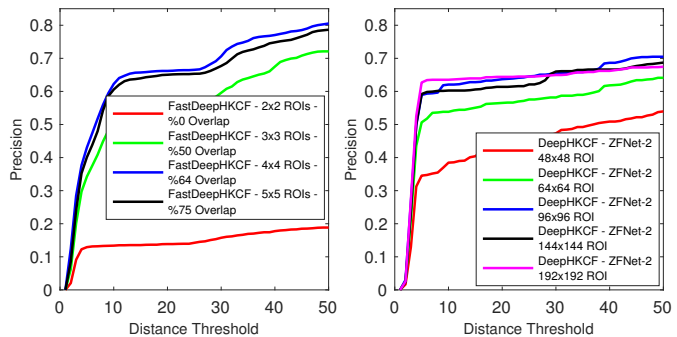
TABLE IV: Comparison of the DeepHKCF tracker to the other hyperspectral template-matching based trackers. The "*" denotes the tracker tested on the same scene from a *fixed* platform. The 6D, 5D and 2D refer to the number of past frames considered in the multi-dimensional assignment algorithm [55]. The use of a *multi-dimensional assignment* algorithm and a *non-linear Bayes Filter* is the key to achieve persistent tracking in the occlusion-dominated scenes. The experiments are carried out on a CPU with 8GB RAM and 2.9GHz i5 processor.

The detection module uses every five neighboring channels to get the heat map of the ROI (200x200 px), resulting in 12 heat maps (61 channels). The heat maps are fused with adaptive coefficients to get a final smoothed heat map. In the final stage, they extract the blobs from the final map and update the track statistics in the past N frames using the multi-dimensional assignment algorithm [55]. The tracker module updates the state space matrix components of the Gaussian Mixture Filter using the new observations in the past N frames. Finally, [5] (HFT) relies on off-line trained road and car classifiers to optimize the search space (200x200 px). The hyperspectral histograms are then computed in a sliding window to assign similarity scores. To optimize the feature extraction step, the integral image theorem [56] is used to compute histogram for each channel in $O(3)$. The heat map is then thresholded and post-processed to find the blobs. The assignment and Bayes Filter modules are similar to [6]. The comparison of the DeepHKCF tracker with those trackers is shown in the table IV. We want to highlight that we exclude the HFT in table IV as it relies on vehicle and asphalt classifiers trained on the samples from the same scene. Such frameworks are limited to similar scenes and may deliver optimistic results.

As seen in table IV, the use of a Bayes Filter and the multi-dimensional assignment algorithm (MDA) is crucial in a scenario largely dominated by occlusions where discriminative trackers-alone are more likely to fail. We believe that the integration of those modules into the DeepHKCF tracker can improve tracking in similar scenarios. One can see the effect of reducing the length of the time window in MDA in both HFAT and HFT tracker. Going from 6-D to 2-D window decreases the precision by 40% for the HFAT. Interestingly, in the *fixed platform* scenario, the HFAT tracker with 2D assignment algorithm performs similarly to the DeepHKCF trackers tested on the *moving platform* scenario. Similarly, the HFT's performance drops drastically by reducing the width of the time window considered in MDA from 5-D to 2-D, especially for the scenario with *trees*. On the other hand, the proposed DeepHKCF trackers outperform HLT in the no-trees scenario by about 30% in terms of central location error. Also, the FastDeepHKCF delivers a slightly faster tracker than the HLT and its individual ROI operations can be easily parallelized whereas the HLT is a more serialized algorithm.

F. Effect of Overlap Ratio in Single KCF-Multiple ROIs Approach

We experiment on the DeepHKCF tracker with ROI mapping (FastDeepHKCF) as a function of the *overlap ratio* between the adjacent ROIs. As mentioned before, it is necessary to have overlap between the adjacent ROIs as the hanning window is applied to the features before the FFT operation. The hanning window filters the noise at the boundaries resulting from FFT operation. Increasing overlap ratio, at the same time, leads to increased complexity ($O(m * n \log(n))$) due to a larger number of ROIs (m) in the full ROI (96x96 px). Fig. 9a shows the precision rates of FastDeepHKCF tracker with different overlap ratios between the adjacent ROIs.



(a) Varying overlap ratio between ROIs in FastDeepHKCF (b) Varying full ROI size in DeepHKCF

Fig. 9: The FastDeepHKCF tracker is experimented on the *no-trees* scenario with varying overlap ratio in the single KCF-multiple ROIs approach (a) whereas (b) shows the results on the effect of different full ROI sizes in DeepHKCF. In (b), the trackers are run through the first 25 frames of each target on the *scenario with trees*.

The 64% and 75% overlap ratios lead to drastically better results than the lower ones (fig. 9a), however, considering the accuracy/speed trade-off, the 64% overlap ($m = 16$) setting delivers the optimal tracker.

G. Effect of ROI Size

The overlap between the adjacent ROIs is an essential part of the DeepHKCF tracker as it ensures consideration

of the every single point in the full ROI by the correlation filter. Another key parameter in this direction is the full ROI size since we have a low temporal resolution and occlusion-dominated scene. We enlarge the ROI size of the optimal DeepHKCF tracker and observe the performance in the *scene with trees*. The results are shown in fig. 9b. In this experiment, the run-time performance of the tracker is ignored as the goal is to measure the contribution of full ROI size.

As shown in fig. 9b, the larger ROI size with the same overlap ratio does not necessarily lead to better performance while quadratically reducing the speed. We believe this is mainly due to growing confusion as the larger ROIs contain a higher number of similar objects. Additionally, these results demonstrate the obvious need to couple the tracking-by-detection algorithms to a Multi-dimensional Assignment algorithm in a Bayes Filter framework in occlusion-dominated scenes [6], [5], [4].

VII. CONCLUSION

Adaptive multi-modal sensors are becoming increasingly important in the aerial tracking domain due to the unique challenges posed by this platforms. In this study, we propose a tracking-by-detection algorithm driven tracker inspired by a multi-modal sensor and deep features. This approach replaces the traditional template-matching based hyperspectral trackers with a new state-of-the-art tracker becoming increasingly popular in traditional visual object tracking. More specifically, we delivered a new framework to handle low temporal resolution in aerial platforms in KCF tracker, called *single KCF-multiple ROIs approach*. To further boost the tracking accuracy, we replaced the traditional features with deep CNN features. Finally, an ROI mapping approach was proposed to speed up extracting features in a single KCF-multiple ROIs approach. The proposed DeepHKCF tracker was evaluated on synthetic scenarios generated by *DIRSIG* software. In the scenario with no-trees, the DeepHKCF tracker performs exceptionally well with 80% precision at 50 px, outperforming other template-matching based trackers. In the same scenario but dominated by occlusions, it is outperformed by the trackers employing a *multi-dimensional assignment algorithm* and *Bayes Filter*. To prove the high-fidelity of the *DIRSIG* generated scenarios, we build a synthetic, aerial vehicle classification dataset to perform classification on the real-platform (*WAMI*). Our dataset, consisting of 55226 samples, was used to train CNNs to perform binary classification. We achieve about 93.2% on the *WAMI* samples by only training on synthetic dataset. This dataset can be highly beneficial in aerial detection and tracking due to limited amount of publicly available data in those domains.

In future work, we plan on supporting the DeepHKCF tracker by integrating a multi-dimensional assignment algorithm and Bayes Filter to better handle severe occlusions. Also, we want to extend the proposed single KCF-multiple ROIs tracking strategy to adopt a more advanced correlation filter tracker such as ECO.

REFERENCES

- [1] R. Pelapur, S. Candemir, F. Bunyak, M. Poostchi, G. Seetharaman, and K. Palaniappan, "Persistent target tracking using likelihood fusion in wide-area and full motion video sequences," in *Information Fusion (FUSION), 2012 15th International Conference on*. IEEE, 2012, pp. 2420–2427.
- [2] J. Portmann, S. Lynen, M. Chli, and R. Siegwart, "People detection and tracking from aerial thermal views," in *Robotics and Automation (ICRA), 2014 IEEE International Conference on*. IEEE, 2014, pp. 1794–1800.
- [3] M. Danelljan, G. Bhat, F. S. Khan, and M. Felsberg, "Eco: Efficient convolution operators for tracking," *arXiv preprint arXiv:1611.09224*, 2016.
- [4] B. Uz Kent, M. J. Hoffman, and A. Vodacek, "Efficient integration of spectral features for vehicle tracking utilizing an adaptive sensor," in *IS&T/SPIE Electronic Imaging*, 2015, pp. 940 707–940 707.
- [5] B. Uz Kent, *Real-time Aerial Vehicle Detection and Tracking using a Multi-modal Optical Sensor*. Rochester Institute of Technology, 2016.
- [6] B. Uz Kent, A. Rangnekar, and M. J. Hoffman, "Aerial vehicle tracking by adaptive fusion of hyperspectral likelihood maps," in *Computer Vision and Pattern Recognition Workshops (CVPRW), 2017 IEEE Conference on*. IEEE, 2017, pp. 233–242.
- [7] AFRL, "Wright-patterson air force base (wpafb) dataset," <https://www.sdms.afrl.af.mil/index.php?collection=wpafb2009>, 2009.
- [8] —, "Wami columbus large image format (clif) dataset," <https://www.sdms.afrl.af.mil/index.php?collection=clif2007>, 2007.
- [9] O. Russakovsky, J. Deng, H. Su, J. Krause, S. Satheesh, S. Ma, Z. Huang, A. Karpathy, A. Khosla, M. Bernstein *et al.*, "Imagenet large scale visual recognition challenge," *International Journal of Computer Vision*, vol. 115, no. 3, pp. 211–252, 2015.
- [10] B. Uz Kent, M. J. Hoffman, and A. Vodacek, "Integrating Hyperspectral Likelihoods in a Multidimensional Assignment Algorithm for Aerial Vehicle Tracking," *IEEE Journal of Selected Topics in Applied Earth Observations and Remote Sensing*, vol. 9, no. 9, pp. 4325–4333, 2016.
- [11] F. Darema, "Dynamic data driven applications systems: A new paradigm for application simulations and measurements," *Computational Science-ICCS 2004*, pp. 662–669, 2004.
- [12] J. F. Henriques, R. Caseiro, P. Martins, and J. Batista, "High-speed tracking with kernelized correlation filters," *IEEE Transactions on Pattern Analysis and Machine Intelligence*, vol. 37, no. 3, pp. 583–596, 2015.
- [13] S. Hare, S. Golodetz, A. Saffari, V. Vineet, M.-M. Cheng, S. L. Hicks, and P. H. Torr, "Struck: Structured output tracking with kernels," *IEEE transactions on pattern analysis and machine intelligence*, vol. 38, no. 10, pp. 2096–2109, 2016.
- [14] Z. Kalal, K. Mikolajczyk, and J. Matas, "Tracking-learning-detection," *IEEE transactions on pattern analysis and machine intelligence*, vol. 34, no. 7, pp. 1409–1422, 2012.
- [15] R. LaLonde, D. Zhang, and M. Shah, "Fully convolutional deep neural networks for persistent multi-frame multi-object detection in wide area aerial videos," *arXiv preprint arXiv:1704.02694*, 2017.
- [16] M. Yi, F. Yang, E. Blasch, C. Sheaff, K. Liu, G. Chen, and H. Ling, "Vehicle classification in wami imagery using deep network," in *SPIE Defense+ Security*. International Society for Optics and Photonics, 2016, pp. 98 380E–98 380E.
- [17] E. J. Lentilucci and S. D. Brown, "Advances in wide-area hyperspectral image simulation," in *AeroSense 2003*. International Society for Optics and Photonics, 2003, pp. 110–121.
- [18] J. F. Henriques, R. Caseiro, P. Martins, and J. Batista, "Exploiting the circulant structure of tracking-by-detection with kernels," in *Proceedings on European Conference on Computer Vision*, 2012, pp. 702–715.
- [19] R. Collins, X. Zhou, and S. K. Teh, "An open source tracking testbed and evaluation web site."
- [20] M. Mueller, N. Smith, and B. Ghanem, "A benchmark and simulator for uav tracking," in *Proceedings of European Conference on Computer Vision*, 2016, pp. 445–461.
- [21] L. W. Sommer, M. Teutsch, T. Schuchert, and J. Beyerer, "A survey on moving object detection for wide area motion imagery," in *Applications of Computer Vision (WACV), 2016 IEEE Winter Conference on*. IEEE, 2016, pp. 1–9.
- [22] M. Teutsch and M. Grinberg, "Robust detection of moving vehicles in wide area motion imagery," in *Proceedings of the IEEE Conference on Computer Vision and Pattern Recognition Workshops*, 2016, pp. 27–35.
- [23] M. Cormier, L. W. Sommer, and M. Teutsch, "Low resolution vehicle re-identification based on appearance features for wide area motion imagery," in *2016 IEEE Winter Applications of Computer Vision Workshops (WACVW)*. IEEE, 2016, pp. 1–7.

- [24] B. Uz Kent, M. J. Hoffman, A. Vodacek, J. P. Kerekes, and B. Chen, "Feature matching and adaptive prediction models in an object tracking dddas," *Procedia Computer Science*, vol. 18, pp. 1939–1948, 2013.
- [25] B. Uz Kent, M. J. Hoffman, A. Vodacek, and B. Chen, "Feature matching with an adaptive optical sensor in a ground target tracking system," *IEEE Sensors Journal*, vol. 15, no. 1, pp. 510–519, 2015.
- [26] R. D. Meyer, K. J. Kearney, Z. Ninkov, C. T. Cotton, P. Hammond, and B. D. Statt, "RITMOS: a micromirror-based multi-object spectrometer," in *SPIE Astronomical Telescopes+ Instrumentation*. International Society for Optics and Photonics, 2004, pp. 200–219.
- [27] S. Han, A. Fafard, J. Kerekes, M. Gartley, E. Ientilucci, A. Savakis, C. Law, J. Parhan, M. Turek, K. Fieldhouse *et al.*, "Efficient generation of image chips for training deep learning algorithms," in *Automatic Target Recognition XXVII*, vol. 10202. International Society for Optics and Photonics, 2017, p. 1020203.
- [28] S. Han and J. P. Kerekes, "Overview of passive optical multispectral and hyperspectral image simulation techniques," *IEEE Journal of Selected Topics in Applied Earth Observations and Remote Sensing*, 2017.
- [29] B. Uz Kent, M. J. Hoffman, and A. Vodacek, "Spectral validation of measurements in a vehicle tracking dddas," *Procedia Computer Science*, vol. 51, pp. 2493–2502, 2015.
- [30] B. Uz Kent, M. J. Hoffman, A. Vodacek, and B. Chen, "Background image understanding and adaptive imaging for vehicle tracking," in *SPIE Defense+ Security*. International Society for Optics and Photonics, 2015, pp. 94 600F–94 600F.
- [31] H. K. Galoogahi, T. Sim, and S. Lucey, "Multi-channel correlation filters," in *Proceedings of International Conference on Computer Vision*, 2013.
- [32] M. Tang and J. Feng, "Multi-kernel correlation filter for visual tracking," in *Proceedings of International Conference on Computer Vision*, 2015, pp. 3038–3046.
- [33] C. Ma, X. Yang, C. Zhang, and M.-H. Yang, "Long-term correlation tracking," in *Proceedings of the IEEE Conference on Computer Vision and Pattern Recognition*, 2015, pp. 5388–5396.
- [34] A. Bibi and B. Ghanem, "Multi-template scale-adaptive kernelized correlation filters," in *Proceedings of the IEEE International Conference on Computer Vision Workshops*, 2015, pp. 50–57.
- [35] Y. Li and J. Zhu, "A scale adaptive kernel correlation filter tracker with feature integration," in *European Conference on Computer Vision*. Springer, 2014, pp. 254–265.
- [36] N. Dalal and B. Triggs, "Histograms of oriented gradients for human detection," in *Computer Vision and Pattern Recognition, 2005. CVPR 2005. IEEE Computer Society Conference on*, vol. 1. IEEE, 2005, pp. 886–893.
- [37] P. F. Felzenszwalb, R. B. Girshick, D. McAllester, and D. Ramanan, "Object detection with discriminatively trained part-based models," *IEEE transactions on pattern analysis and machine intelligence*, vol. 32, no. 9, pp. 1627–1645, 2010.
- [38] D. S. Bolme, J. R. Beveridge, B. A. Draper, and Y. M. Lui, "Visual object tracking using adaptive correlation filters," in *Computer Vision and Pattern Recognition (CVPR), 2010 IEEE Conference on*. IEEE, 2010, pp. 2544–2550.
- [39] A. Krizhevsky, I. Sutskever, and G. E. Hinton, "Imagenet classification with deep convolutional neural networks," in *Advances in neural information processing systems*, 2012, pp. 1097–1105.
- [40] K. Simonyan and A. Zisserman, "Very deep convolutional networks for large-scale image recognition," *arXiv preprint arXiv:1409.1556*, 2014.
- [41] C. Szegedy, W. Liu, Y. Jia, P. Sermanet, S. Reed, D. Anguelov, D. Erhan, V. Vanhoucke, and A. Rabinovich, "Going deeper with convolutions," in *Proceedings of the IEEE conference on computer vision and pattern recognition*, 2015, pp. 1–9.
- [42] M. Danelljan, G. Hager, F. Shahbaz Khan, and M. Felsberg, "Convolutional features for correlation filter based visual tracking," in *Proceedings of the IEEE International Conference on Computer Vision Workshops*, 2015, pp. 58–66.
- [43] L. Wang, T. Liu, G. Wang, K. L. Chan, and Q. Yang, "Video tracking using learned hierarchical features," *IEEE Transactions on Image Processing*, vol. 24, no. 4, pp. 1424–1435, 2015.
- [44] D. Held, S. Thrun, and S. Savarese, "Learning to track at 100 fps with deep regression networks," in *European Conference on Computer Vision*. Springer, 2016, pp. 749–765.
- [45] L. Bertinetto, J. Valmadre, J. F. Henriques, A. Vedaldi, and P. H. Torr, "Fully-convolutional siamese networks for object tracking," in *European Conference on Computer Vision*. Springer, 2016, pp. 850–865.
- [46] L. Leal-Taixé, C. Canton-Ferrer, and K. Schindler, "Learning by tracking: Siamese cnn for robust target association," in *Proceedings of the IEEE Conference on Computer Vision and Pattern Recognition Workshops*, 2016, pp. 33–40.
- [47] R. Girshick, "Fast r-cnn," in *Proceedings of the IEEE international conference on computer vision*, 2015, pp. 1440–1448.
- [48] S. Ren, K. He, R. Girshick, and J. Sun, "Faster r-cnn: Towards real-time object detection with region proposal networks," in *Advances in neural information processing systems*, 2015, pp. 91–99.
- [49] J. Dai, Y. Li, K. He, and J. Sun, "R-fcn: Object detection via region-based fully convolutional networks," in *Advances in neural information processing systems*, 2016, pp. 379–387.
- [50] F. Yu and V. Koltun, "Multi-scale context aggregation by dilated convolutions," *arXiv preprint arXiv:1511.07122*, 2015.
- [51] Y. Jia, E. Shelhamer, J. Donahue, S. Karayev, J. Long, R. Girshick, S. Guadarrama, and T. Darrell, "Caffe: Convolutional architecture for fast feature embedding," *arXiv preprint arXiv:1408.5093*, 2014.
- [52] J. Redmon and A. Farhadi, "Yolo9000: better, faster, stronger," *arXiv preprint arXiv:1612.08242*, 2016.
- [53] W. Liu, D. Anguelov, D. Erhan, C. Szegedy, S. Reed, C.-Y. Fu, and A. C. Berg, "Ssd: Single shot multibox detector," in *European conference on computer vision*. Springer, 2016, pp. 21–37.
- [54] R. Kemker and C. Kanan, "Deep neural networks for semantic segmentation of multispectral remote sensing imagery," *arXiv preprint arXiv:1703.06452*, 2017.
- [55] A. B. Poore, "Multidimensional assignment formulation of data association problems arising from multitarget and multisensor tracking," *Computational Optimization and Applications*, vol. 3, no. 1, pp. 27–57, 1994.
- [56] F. Porikli, "Integral histogram: A fast way to extract histograms in cartesian spaces," in *Computer Vision and Pattern Recognition, 2005. CVPR 2005. IEEE Computer Society Conference on*, vol. 1. IEEE, 2005, pp. 829–836.